AXIAL SHORTENING OF STEEL COLUMNS IN BUILDINGS SUBJECTED TO EARTHQUAKES

Gregory A. MacRae[1], Christopher R. Urmson[2], Warren R. Walpole[1], Peter Moss[1], Karissa Hyde[3] and Charles Clifton[4]

ABSTRACT

Steel members subject to axial compression and inelastic cyclic displacements, such as may occur during earthquake excitation, exhibit axial shortening due to material inelastic deformation irrespective of the occurrence of buckling. This column axial shortening can cause undesirable effects in the building, especially if it occurs to a different extent in different columns of a seismic-resisting system. This paper summarizes experimental and finite element studies to quantify the axial shortening of columns with known axial forces pushed to inelastic cyclic displacements. A flexural hinge model for a frame analysis program is developed and calibrated against that from experimental and analytical studies. Then, to quantify the effect of axial shortening on realistic moment and eccentrically-braced frames during earthquakes, inelastic dynamic time history analyses were conducted. While axial shortening of more than 7% of the column length was obtained during experimental testing, the axial shortening was always less than 1% of the column interstorey height in the steel frames studied. A method to estimate the axial shortening as a function of the expected inelasticity is developed. Finally, several new details are described in order to prevent detrimental effects due to axial shortening.

1. INTRODUCTION

Steel moment-resisting frames (MRFs) and eccentrically-braced frames (EBFs) are commonly used in seismic regions of the world. Although steel code provisions (e.g. SNZ, 1997) tend to discourage yielding of columns over the frame height using capacity design considerations, significant yielding may occur in the columns at ground level. This cyclic yielding may cause significant column axial shortening for the reasons described below.

Consider the cantilever column in Figure 1. As the column top translates laterally, it induces a bending moment at the column base. Stresses resulting from this moment, and from axial compression, combine. If the yield stress of the column is exceeded, and inelastic action occurs, the stress distribution is shown in Figure 1a, where the neutral axis of the section is on the tension side and the centre of the column may be yielding in compression. When the column top is displaced in the reverse direction, the neutral axis migrates toward the opposite side of the section, as shown in Figure 1b. Again, the centre of the section yields in compression causing the column to shorten. Further cyclic lateral displacement, as shown in Figure 1c, causes the axial shortening which will be dependent on both the magnitude of the inelastic cycles, as well as on the number of inelastic loading cycles. It may be seen that inelastic axial shortening is related to material nonlinearity, and while it may be exacerbated by buckling, it can occur independently of whether or not buckling occurs. While Figure 1 provides a simple physical understanding for axial shortening, the actual shortening mechanism is more complex than this as a result of residual stresses in the section, non-elastic perfectly plastic (EPP) material stress-strain curves and load path dependence of the stresses.

The only experiments known on steel columns which specifically reported axial shortening were carried out by MacRae *et al.* (1990). Here, 250UC73 columns were tested under constant axial compression and reverse cyclic displacement causing bending about the column strong axis. The columns had constant axial force ratios, P/P_y, of 0.0, 0.3, 0.4, 0.5, 0.6, 0.7 and 0.8 respectively. These columns are referred to as columns C*x*, where *x* is 10 times the axial force ratio. For example, C5 had an axial force ratio of 0.50. An additional column was subject to a varying axial force ratio to represent the likely forces on the exterior column of a frame. Testing was carried out using the configuration in Figure 2. Here the top and bottom were held in place laterally at the pins shown. When the loading ram was extended, the 530UB82 load frame rotated about the bottom pin thereby applying lateral force to the column. At the beginning of testing, axial force was applied to the columns. Then the columns were subject to cyclic lateral displacements with two cycles to member displacement ductilities of 2, 4, 6, 8 and 10.

Lateral force-displacement plots and axial shortening plots are given in Figures 3 and 4 for columns with axial force ratios of 0.0 and 0.5 respectively. Column C0, has quite a stable lateral force displacement plot. For higher axial forces, there was strength degradation as shown in Figure 3b due to large

[1] *Department of Civil and Natural Resources Engineering, University of Canterbury, Christchurch*

[2] *Zachry Department of Civil Engineering, Texas A & M University, College Station, Texas, USA*

[3] *MWH Global, Christchurch, New Zealand*

[4] *Department of Civil and Environmental Engineering, University of Auckland, Auckland*

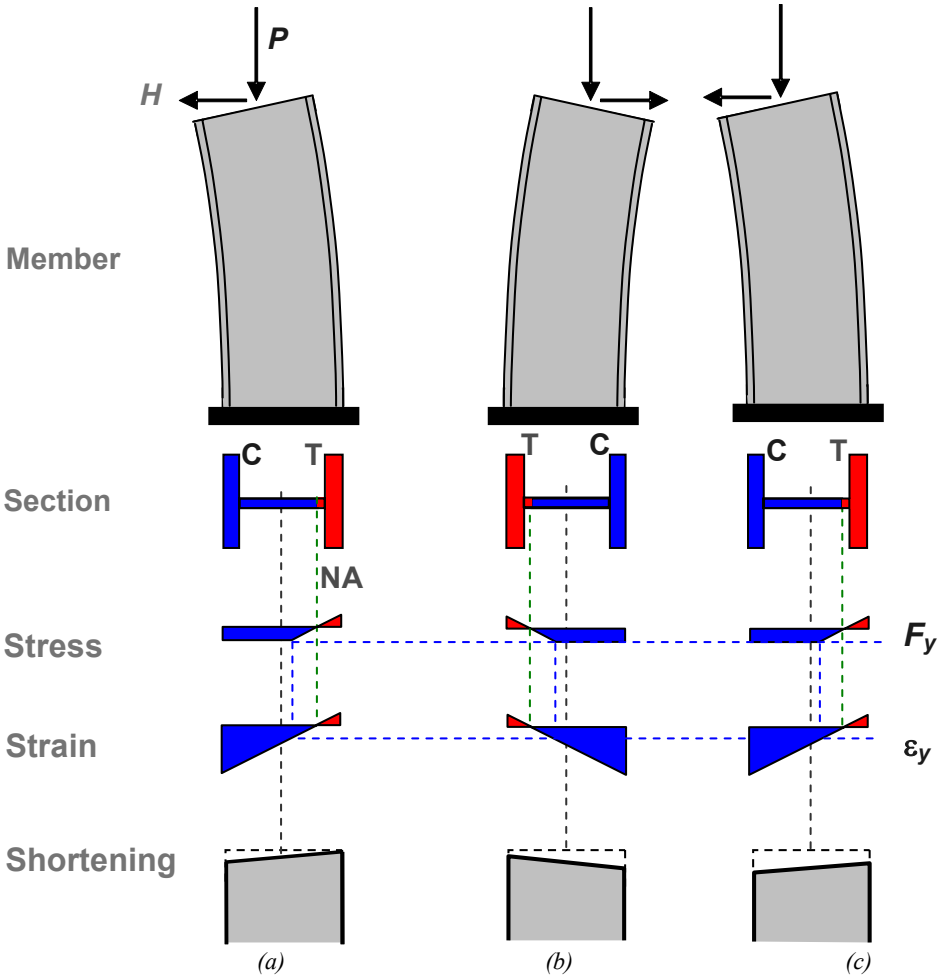

Figure 1: Axial Shortening Mechanism.

amounts of local buckling which was accentuated by the lateral buckling. The axial deformation of column C0, with only a small compressive force of 20 kN to hold the column in place, was expected to be almost zero since the neutral axis was expected to remain at the centre of the section. Instead, a small amount (less than 1 mm) of axial extension may be observed in Figure 4a. This may be explained by the test configuration where any lateral force causes a component of tension in the column at the maximum displacement in both directions. Poisson's ratio effects are also consistent with this observation. The amount of axial shortening in Column C5 is substantial being about 85 mm. This is about 7.7% over the height. This sort of deformation is likely to be unacceptable in a real building.

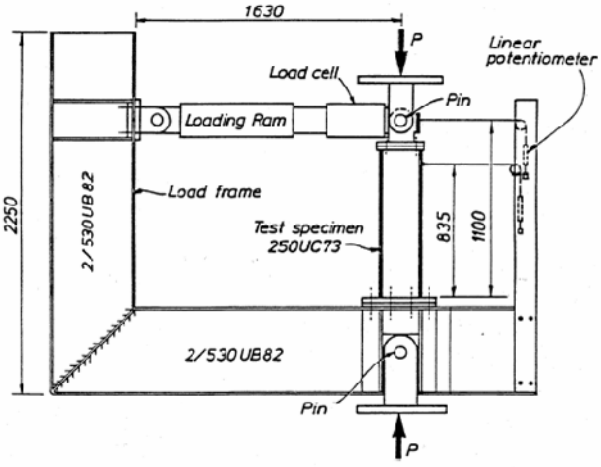

Figure 2: Test Configuration for Steel Column.

In order to estimate the likely magnitude of axial shortening it can be assumed that both the magnitude and number of inelastic loading cycles are important as described in the idealization associated with Figure 1. The axial shortening is plotted against cumulative inelastic rotation, $\Sigma\theta_H$, in Figure 5. It may be seen that the relationship is initially linear, but at large $\Sigma\theta_H$, the axial shortening rate increases as a result of section buckling. Also, the initial rate of axial shortening is the same for high axial force ratios.

The cumulative inelastic rotation, $\Sigma\theta_H$, used in Figure 5 is given in Equation 1 as a function of the rotation at the initiation of plasticity, θ_p, which is computed as the plastic displacement at the point of inflection, δ_p, divided by the distance from the critical section to the point of inflection, L, and the cumulative inelastic ductility, $\Sigma\mu_H$. The cumulative inelastic ductility, $\Sigma\mu_H$, is calculated as the sum of the absolute inelastic ductilities in each direction. This is shown in Figure 6 using an elastic perfectly plastic (EPP) hysteresis loop, and in Figure 7 for the loading regime used in the testing.

$$\Sigma\theta_H = \frac{\Sigma\mu_H \delta_p}{L} \qquad (1)$$

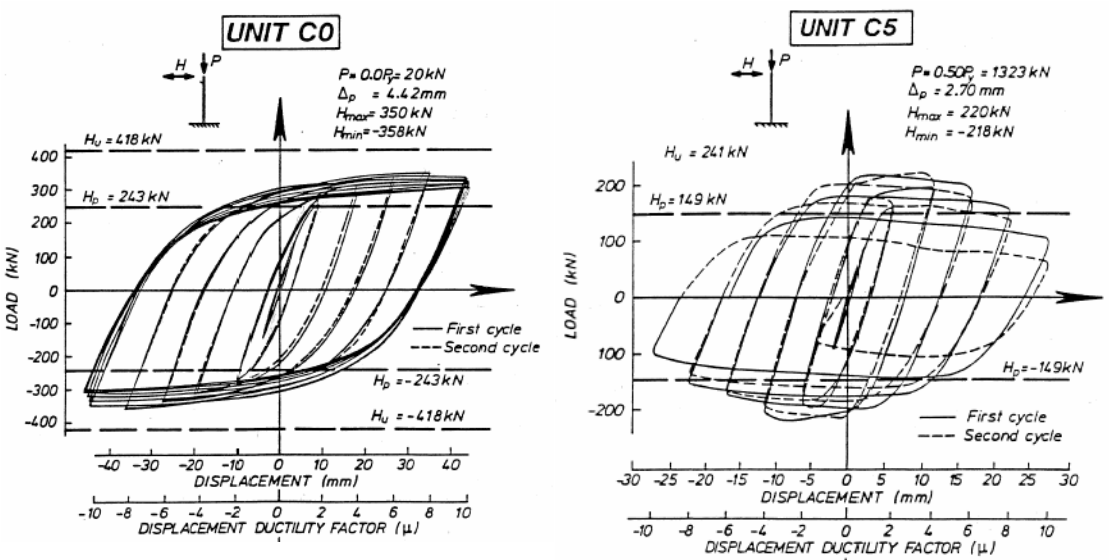

(a) Axial force ratio, P/P_y, of 0.0 *(b) Axial force ratio, P/P_y, of 0.5*

Figure 3: Horizontal Force-Displacement Hysteretic Loops.

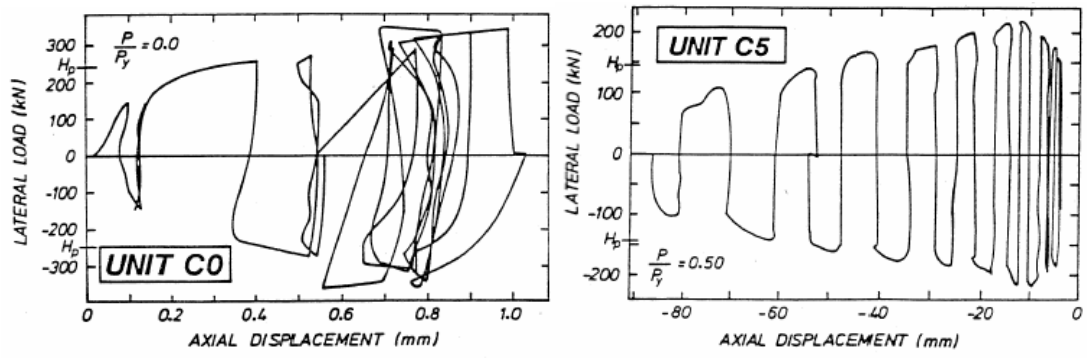

(a) Axial force ratio, P/P_y, of 0.0 *(b) Axial force ratio, P/P_y, of 0.5*

Figure 4: Horizontal Force-Axial Deformation Plots.

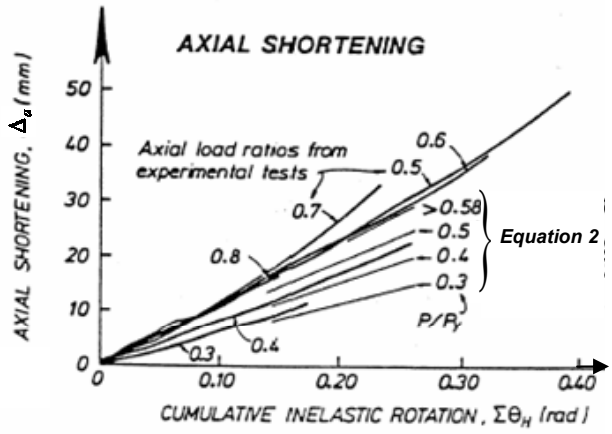

Figure 5: Shortening and Cumulative Inelastic Rotation Relationship (MacRae, 2005).

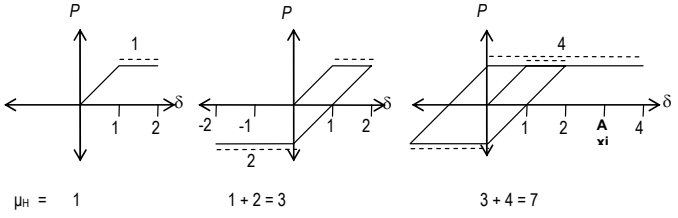

Figure 6: EPP Model Showing Cumulative Inelastic Ductility Calculation.

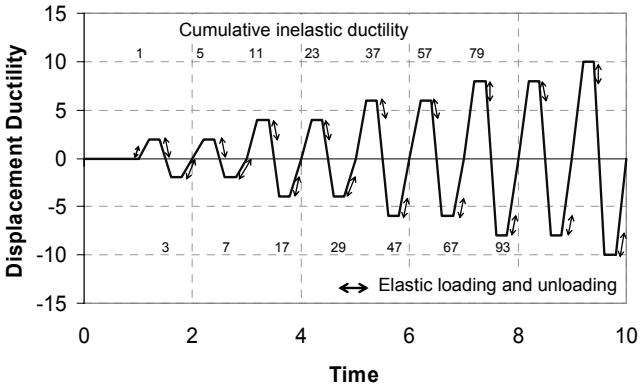

Figure 7: Loading Regime Showing Cumulative Inelastic Ductility for Member Displacement Ductility.

An empirical relationship between cumulative inelastic rotation, $\Sigma\theta_H$, and axial shortening, Δ_a, was developed for the linear portion of the curve in Figure 5 as shown in Equation 2 (MacRae et al. 1990).

$$\Delta_a = -0.446\frac{P}{2.54P_y}\frac{A}{A_w}L_p\Sigma\theta_H \quad \text{for} \quad \frac{P}{P_y} \le \frac{2.54A_w}{A} \qquad (2)$$
$$= -0.446L_p\Sigma\theta_H \quad \text{for} \quad \frac{P}{P_y} > \frac{2.54A_w}{A}$$

Here L_p is the plastic hinge length, which was taken as the member depth, D. The parameter $PA/(P_yA_w)$ would be less than unity, when the neutral axis is in the web of the section, if the material behaviour were truly elastic-perfectly plastic (EPP). In this case the axial shortening is dependent on the axial force ratio, P/P_y. When the axial force ratio is zero, the neutral axis is in the centre of the section and no axial shortening is expected, but when $PA/(P_yA_w) = 1$ (i.e. $P/P_y = A_w/A$) the neutral axis is in the flange. A factor of 2.54 is used to fit the experimental results at low axial forces. It adjusts the axial force causing the neutral axis to be in the flange as a result of the non-EPP material stress-strain relationship. For high axial force ratios, the degree of axial shortening appears to be independent of the axial force ratio, because the neutral axis is in the column flange. In this case, there is only a small change in strain at the centre of the section, ε_c, due to a change in axial force as shown in Figure 8. As a result of buckling, the curves in Figure 5 become increasingly non-linear at higher values of cumulative inelastic rotation.

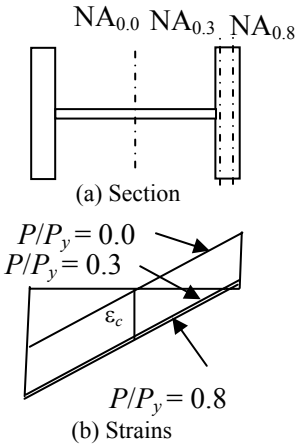

Figure 8: Position of NA with Different AxialForce Ratios, P/P_y

Hopperstad and Remseth (1996) showed that a finite element model could describe the lateral force-displacement behaviour of the columns tested above well, but they did not discuss axial shortening. The only known study carried out to analytically investigate axial shortening of columns due to reverse cyclic displacements was by Hyde *et al.* (2006). The finite element programme ABAQUS (2004) was used to model the seven columns tested experimentally as described above. Among other findings, it was shown that Equation 2 could be superseded because the amount of axial shortening is independent of the plastic hinge length L_p as shown in Equation 3 for monotonic loading, if the neutral axis is in one flange.

$$\begin{aligned}\Delta_a &= \varepsilon_c L_p \\ &= -\phi L_p D/2 \\ &= \frac{-\theta_H}{L_p}\frac{D}{2}L_p \\ &= -\theta_H D/2\end{aligned} \qquad (3)$$

The revised equation is Equation 4. Again, when the neutral axis is in the flange, the amount of axial shortening appears to be independent of the axial force ratio P/P_y.

$$\Delta_a = \begin{cases} -0.5\dfrac{P}{P_y}\dfrac{A}{A_w}D\Sigma\mu_H\dfrac{\delta_p}{L} & \text{for} \quad \dfrac{P}{P_y} \le \dfrac{A_w}{A} \\ -0.5D\Sigma\mu_H\dfrac{\delta_p}{L} & \text{for} \quad \dfrac{P}{P_y} > \dfrac{A_w}{A} \end{cases} \qquad (4)$$

Equation 4, shown as "*Hyde*", is compared with the finite element model results without buckling effects in Figure 9. The analysis and model developed by Hyde is similar to that of Equation 4 for high axial force ratios, but it predicts greater axial displacements, and is therefore conservative, for low axial force ratios. This is because Equation 4 does not consider the increase in element strength due to large compressive strains. Both the finite element results and Equation 4 predict larger displacements than Equation 2, which is based on the experimental results.

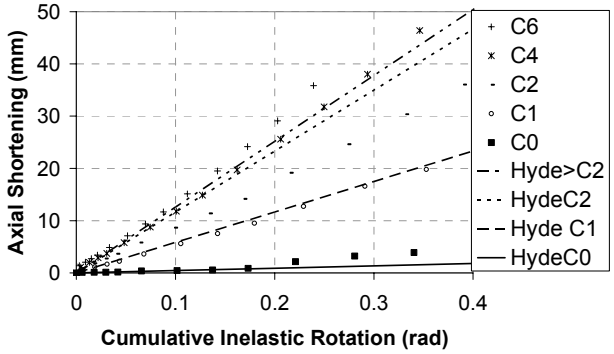

Figure 9: Comparison of Equation 4 with Analytical Results.

From the discussion above, it may be seen that axial shortening has been quantified from experiments, and explained using simplistic theory. Also, application of this theory gives a reasonable estimate of the column shortening under a known loading regime if buckling is not considered. In order to determine whether axial shortening is significant and detrimental for real frames under earthquake shaking, and to have the option of preventing it from becoming a major problem, it is necessary to:

i) develop a column model in a frame analysis program which simulates the axial shortening,
ii) incorporate the column model into realistic building frames which undergo yielding to evaluate the likely effect amount of shortening under realistic shaking, and
iii) consider the possibility of column details which reduce or mitigate the effects of the shortening.

This paper seeks to address the issues above by focussing on the axial shortening behaviour of EBF and MRF frames designed for moderate and high seismic regions.

2. SHORTENING IN FRAME COLUMN MODEL

A multi-spring model of a column able to undergo axial shortening was developed and analysed in Ruaumoko-2D (Carr, 2007) under the same loading regime used for the experimental study and for the finite element analyses. The test set-up, materials and dimensions were the measured values from the experimental study which were also used in the finite element study. Column dimensions are shown in Figure 10. Figure 10a shows an elevation of the column, and Figure 10b shows the section was divided up into sixteen areas, each represented by a spring with the appropriate axial stiffness. Because of the effects of bending, more springs were used in the flanges than in the web. A translational spring was used at mid-height of the section to allow for the shear stiffness of the section over the plastic hinge length. Springs were connected to the base and to the elastic part of the column using rigid links. The columns were modelled as having elastic–perfectly plastic force-displacement behaviour, as this seemed reasonable based on Figure 3b. Special attention was given to the bilinear factor of the hinge fibres. It was made slightly greater than zero to prevent numerical instability and to ensure that the overall member force-displacement relationship was still close to elastic-plastic even when small hinge lengths were used. For the model of the 250UC73 used to verify the analytical results of the axial shortening, an elastic portion of the column was fixed to the top of the plastic hinge zone. Axial load and cyclic displacements were applied to the top of the column, which was unconstrained in-plane. This differed from the experimental model, where a rotation was applied to the rigid frame below the column specimen, and the top of the column where the loads were applied was pinned. Hyde (2006) showed that the method used to apply the load has little effect on the level of axial shortening obtained. A sensitivity study was carried out on shortening considering plastic hinge lengths of 1 mm and 10 mm respectively. It was found that the difference was insignificant thereby corroborating the argument that axial shortening is independent of plastic hinge length as described in Equations 3 and 4. It should be noted that the plastic hinge length is chosen to be small to represent the effect of concentrated plasticity at the end of the member. This is because plastic rotation was computed as the plastic displacement divided by the total member length, so such a representation was necessary to obtain as realistic a comparison as possible.

The analytical results from Ruaumoko-2D (shown as "*Urmson*") are similar to those obtained by Equation 4 (shown as "*Hyde*") in Figure 11. Again, columns with low axial force ratios experience almost no axial shortening, while for columns with high axial force ratios the relationship appears to be independent of axial force ratio. There is only a small difference for columns with axial force ratios greater than 14%, so this model was considered to be sufficient for quantifying axial shortening in columns. However, buckling effects would increase the shortening, while greater yield strengths and post-elastic stiffness would tend to decrease the shortening and these two effects are not considered explicitly in the model.

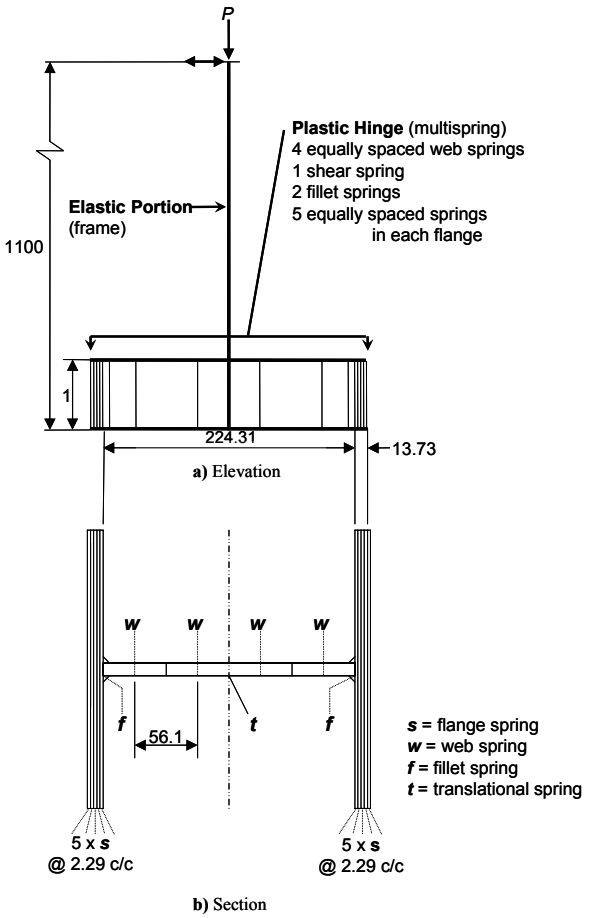

Figure 10: 250UC79 Column Model Showing Dimensions (mm). Not to Scale.

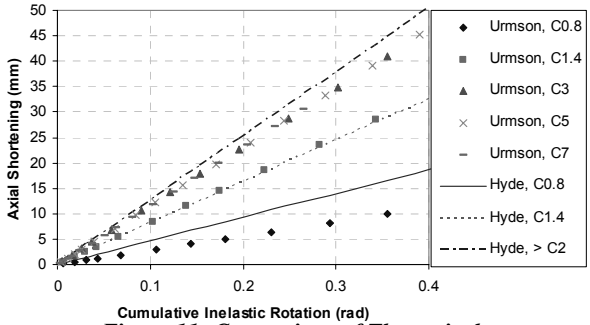

Figure 11: Comparison of Theoretical and Analytical Axial Shortening.

3. SHORTENING DUE TO EARTHQUAKE

Details of four typical structural steel frames expected to sustain significant yielding in the base story were kindly provided by Steel Construction New Zealand (SCNZ). These frames were eccentrically braced frames (EBFs) and moment frames (MFs) designed for Christchurch and Wellington as listed in Table 1 and Figure 12. Christchurch is regarded as a region of moderate seismicity, while Wellington is one of high seismicity. The frames have constant interstorey height unless specified otherwise. All frames were modelled as fully fixed at the base. The seismic weight is given at different levels, *L*, and periods are also provided. Frames 3 and 4 are from orthogonal framing systems in the same building.

For the modelling, Frame 1 columns were fully restrained at the base level at the bottom of the EBF; frame elements were centreline members rigidly connected to each other; frames

Table 1. Frames Analysed

Frame	Location	Frame Type	Storeys	No. Seismic Bays	Seismic Weight (kN)	Period (s)
# 1	Christchurch	EBF	6	1	L1 4180, L2-5 3901, L6 3489	0.945
# 2	Christchurch	MRF	5	1	L1 3417, L2-4 4271, L5 3474	1.71
# 3	Wellington	EBF	5	1	L1-3 1195, L4 1174, L5 1325	0.613
# 4	Wellington	MRF	5	2	L1-3 1195, L4 1174, L5 1325	0.96

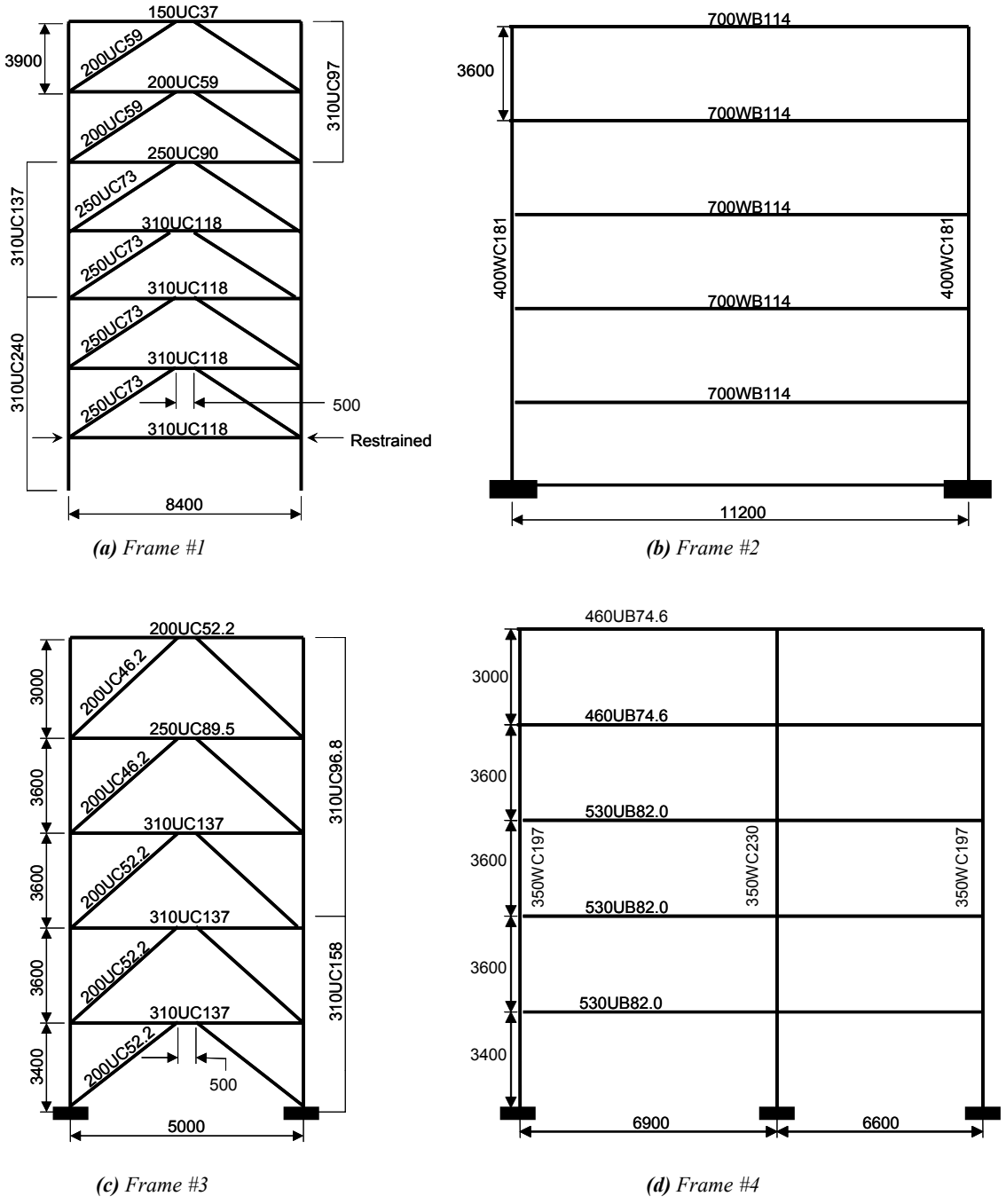

***(a)** Frame #1* ***(b)** Frame #2*

***(c)** Frame #3* ***(d)** Frame #4*

Figure 12: Analytical Frame Models used in Ruaumoko-2D (All dimensions in mm).

were provided with 5% initial stiffness proportional damping in all modes; dead and live loads were applied to frames following New Zealand code provisions (SNZ, 2004) for load combinations under ultimate earthquake loads; each floor seismic weight was distributed evenly between frames acting in the same direction; structural elements were elastic with bilinear plastic hinges at either end; shear links in the EBF were modelled using shear springs as described by Peng *et al.* (2006); all steel members were Grade 300; and the section moment-axial force interaction follows Figure 13, except for the fibre hinges.

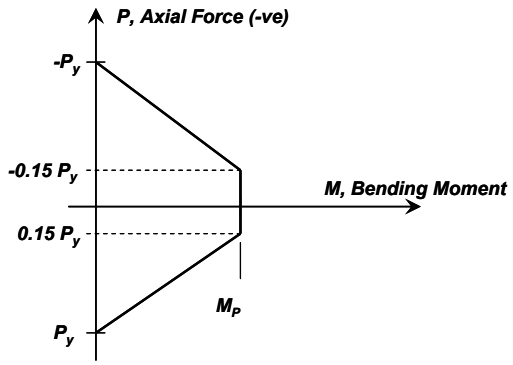

Figure 13: Steel Member Interaction Surface.

Each frame was subjected to a suite of twenty earthquake records taken from the SAC earthquake ground motion record database (Somerville *et al*., 1997). The earthquakes have an exceedance probability of 10% in 50 years for Los Angeles. These earthquake records were scaled to have the same spectral acceleration, at the fundamental period of the structure, as the design basis earthquake (DBE or 500 year event) according to the New Zealand earthquake action provisions (SNZ, 2004). The records were also scaled by 1.8 (SNZ, 2004) to approximately represent ground shaking effects expected in a maximum credible event (MCE) level (2,500 year) event. Time history analysis was conducted with the structural analysis programme Ruaumoko-2D (Carr, 2007) and plastic axial and differential displacements are given in Tables 2 to 5 for the DBE.

The behaviour of the Christchurch MRF (Frame #2) with the scaled LA01 record is shown in Figure 14. This case produces the largest amount of axial shortening of any configuration and it is representative of the behaviour from other analyses. Figure 14a shows that about 31 mm inelastic axial shortening occurred in the left hand column during the first 20 seconds of shaking as the frame moved to the left and the axial force increased in this column as shown in Figures 14b and 14c. The behaviour of the Christchurch EBF (Frame #1) under MCE shaking with the scaled LA01 earthquake record is shown in Figure 15. Plastic axial shortening increases and decreases as shown in Figures 15a and 15b. This is because both tension and compression act on the column as shown in Figures 15c and 15d. The maximum axial shortening was 4.23 mm in the left hand (LH) column and 5.32 mm in the right hand (RH) column. The difference in LH and RH axial shortening 20 seconds through the earthquake record of about 2 mm in the base story corresponds to 4.6 mm roof displacement which is consistent with Figure 15e.

The maximum plastic axial shortening for the column with the maximum shortening in each frame is given in Table 2 for the design level shaking, and in Table 3 for the maximum credible earthquake shaking. These values are the same as those of plastic axial shortening at the end of the analysis for the moment frames which do not yield in tension, but they may be overestimates of the shortening at the end of the analysis for the EBFs (Frames 1 and 3) where axial extension, as well as axial shortening occurs. It may be seen that an average compressive axial displacement of 2.17 mm (0.06% of the story height) was obtained during the design level shaking in the critical column in Frame 2. This is relatively small and it is likely that a building may be fully usable after experiencing such demands. This increased to 3.95 mm (0.11% of the story height) under the MCE. In both cases the effect of buckling is not expected to be severe thereby validating the modelling approach which ignores the buckling effect. The values may be considered to conservatively estimate the axial shortening because the nominal yield strength, without consideration of strain hardening, was used. It may be seen that the EBF axial shortening was relatively small compared to that of these particular moment frames.

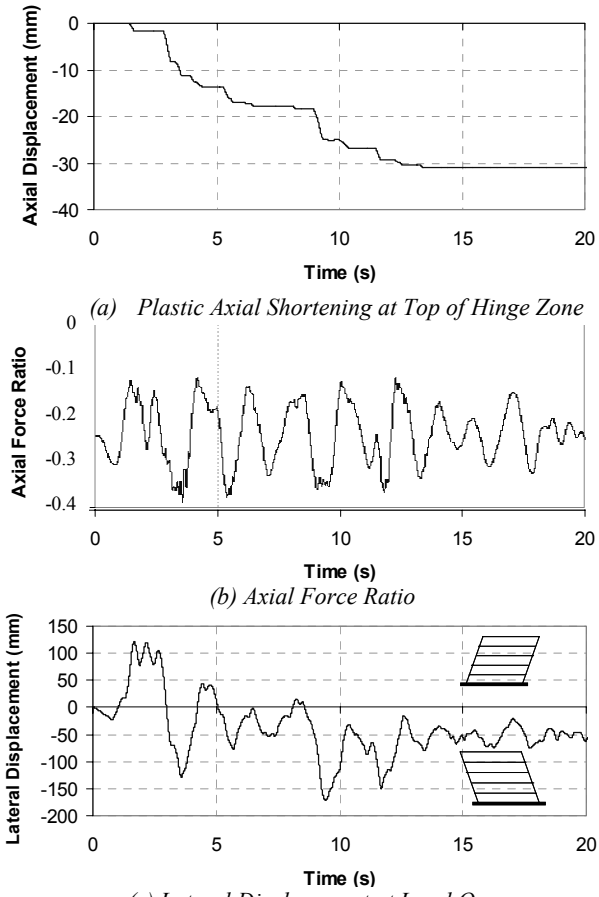

(a) Plastic Axial Shortening at Top of Hinge Zone

(b) Axial Force Ratio

(c) Lateral Displacement at Level One

Figure 14: Left Hand Ground Storey Column Response of Christchurch MRF to Scaled LA01 Record.

The amount of relative displacement at the end of the earthquake record is given for each frame under design basis shaking in Table 4, and under maximum credible shaking in Table 5. The average value of 2.58 mm in Frame 1 during the MCE corresponds to a roof displacement of 2.58 mm x 6 stories x (3.9 m/storey)/(8.4 m bay width) = 7.1 mm. This is a roof drift ratio of 0.3% which is similar to the building construction tolerance of 0.2%.

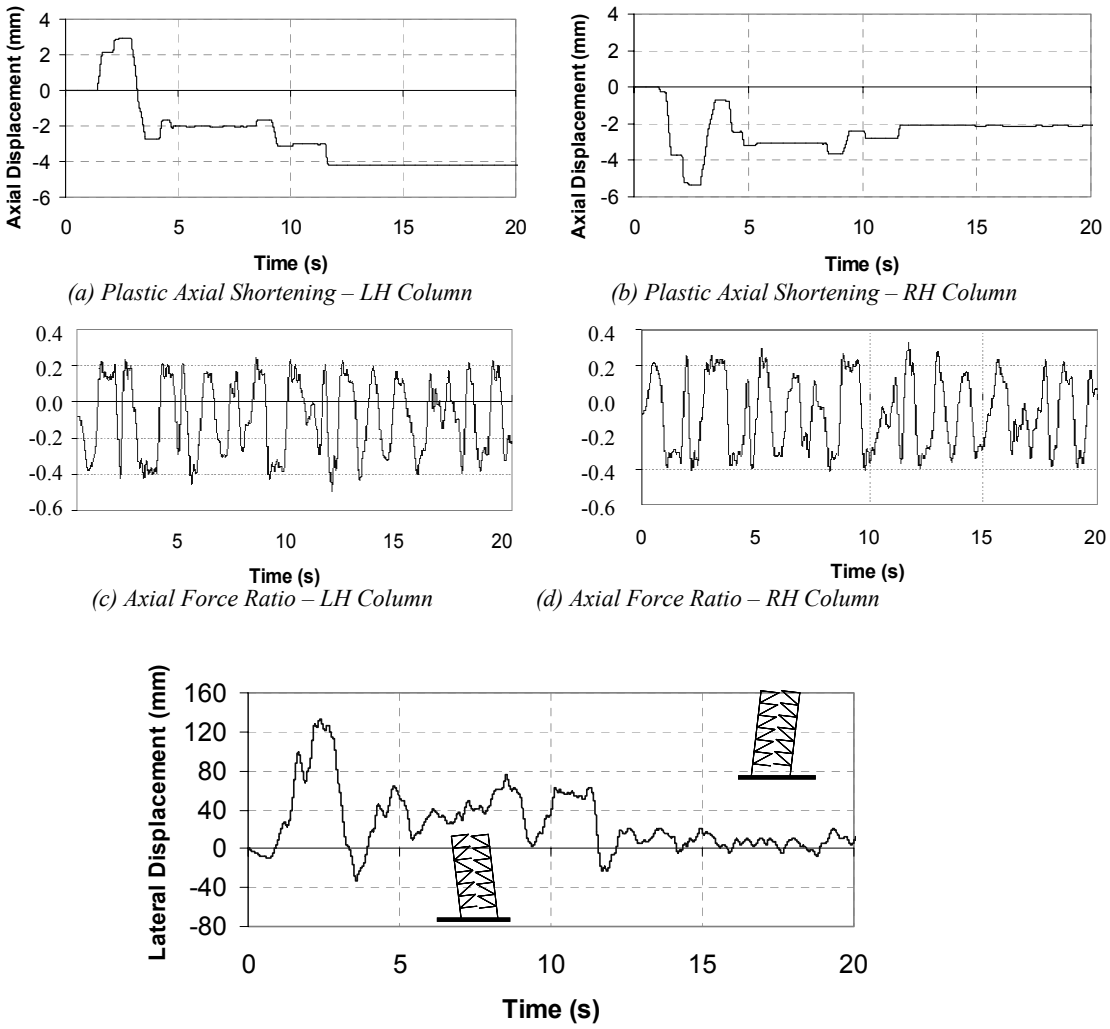

(a) Plastic Axial Shortening – LH Column

(b) Plastic Axial Shortening – RH Column

(c) Axial Force Ratio – LH Column

(d) Axial Force Ratio – RH Column

(e) Lateral Displacement at Roof

Figure 15: Behaviour over Time for Ground Storey Columns in Christchurch EBF under MCE Shaking (LA01 record).

Table 2: Maximum Plastic Axial Shortening (mm) of each Frame under Design Basis Earthquake During Shaking.

	Frame 1 Christchurch EBF	Frame 2 Christchurch MRF	Frame 3 Wellington EBF	Frame 4 Wellington MRF
	Right hand column	Right hand column	Left hand column	Right hand column
Mean	1.81	2.17	0.81	1.80
Std. Dev	0.81	0.24	0.09	0.26

Table 3: Maximum Plastic Axial Shortening (mm) of each Frame under Maximum Credible Earthquake During Shaking.

	Frame 1 Christchurch EBF	Frame 2 Christchurch MRF	Frame 3 Wellington EBF	Frame 4 Wellington MRF
	Right hand column	Right hand column	Left hand column	Right hand column
Mean	2.83	3.95	1.46	3.25
Std. Dev	0.65	0.45	0.17	0.46

Table 4: Absolute Differential Shortening (mm) in Frames under Design Basis Earthquake at the End of the Earthquake Record.

	Frame 1 Christchurch EBF	Frame 2 Christchurch MRF	Frame 3 Wellington EBF	Frame 4 Wellington MRF	
				Left span	Right span
Mean	1.48	1.04	0.11	0.31	0.17
Std. Dev.	3.26	0.95	0.14	0.33	0.19

Table 5: Absolute Differential Shortening (mm) in Frames under Maximum Credible Earthquake at the End of the Earthquake Record.

	Frame 1 Christchurch EBF	Frame 2 Christchurch MRF	Frame 3 Wellington EBF	Frame 4 Wellington MRF	
				Left span	Right span
Mean	2.58	1.54	0.77	1.51	1.14
Std. Dev.	3.36	1.04	0.66	0.98	0.72

4. PREDICTION OF AXIAL SHORTENING

The following methods may be used to estimate the likely column axial shortening during an earthquake.

a) Direct analysis

Direct analysis of building frames may be carried out using the approach described in the previous sections. Here, a fibre hinge model must be developed and time-history analysis of frames can be carried out with a suite of records to estimate the likely demands. Since it is time consuming to properly implement and calibrate the model, simpler and more approximate methods for estimating the demands may be developed as described below.

b) Effective Number of Cycles from SDOF Oscillator

The effective number of cycles of excitation may be found from analyses of single-degree-of-freedom oscillators for a suite of earthquakes and this information may be used in Equation 4. Such a study was performed by MacRae and Kawashima (1993) where eleven different records were used to analyze bilinear oscillators. The equivalent number of cycles, N_c, to any specified peak ductility, μ, was computed as the total hysteretic energy dissipated divided by that dissipated in one full cycle to the peak displacement. The results did not show trends with site soil stiffness, and they were not sensitive to oscillator period when the bilinear factor, r, was less than 0.25. Figure 16a shows that structures with greater ductility are subject to a greater number of cycles, and the number of cycles increases with greater r. For structures in the common range of interest, with r ranging from 0.0 to 0.25 say, it is possible to for an oscillator to experience 4 cycles with high ductilities. Also, if the scatter in results is considered, many more cycles may be appropriate if a reasonable level of confidence is desired as shown in Figure 16b. For a realistic frame it may be difficult to compute the expected cumulative ductility demand of the column, $\Sigma\mu_H$. However, an approximation to the peak ductility, μ, may be obtained as $M_e/M_p(P)$ where M_e is the moment on the column considering the elastic level earthquake without reductions for ductility or special effects, and $M_p(P)$ is the plastic moment capacity considering axial force. The cumulative ductility, $\Sigma\mu_{H1}$, may be obtained for one full cycle according to Equation 5 using the methods described for Figure 6. The cumulative ductility, $\Sigma\mu_H$, is therefore given in Equation 6.

$$\Sigma\mu_{H1} = 4(\mu\text{-}1) \quad (5)$$

$$\Sigma\mu_H = N_c\Sigma\mu_{H1} \quad (6)$$

For example, if the ratio of $M_e/M_p(P)$ is 2.5 for the internal column used in the Christchurch moment frame the ductility, μ, may also be taken as 2.5. For this section the depth is 390 mm and the column web area to total area ratio, A_w/A, is 0.297. The ratio of plastic displacement divided by the height to the point of inflection, δ_p/L, is given by Equation 7. If the total height of the first story is 3.60 m, and the point of inflection is at 0.8 of the column height from the base, then L = 0.8 x 3.60 m = 2.88 m. The plastic moment capacity without reduction for axial force is 1,071 kNm. If the axial force ratio is 0.40, which is greater than A_w/A, then the reduced moment capacity considering the interaction diagram in Figure 13 is 888kNm. Assuming conservatively that the frame has a post-elastic stiffness ratio, r, of 0.25, the average effective number of cycles, N_c, is 3.3, so the cumulative ductility, $\Sigma\mu_H$, is given in Equation 8. The expected axial shortening is 26.5 mm from Equation 9.

$$\frac{\delta_p}{L} = \frac{M_p(P)L}{3EI} = \frac{888kNm \times 2.88m}{3 \times 200GPa \times 620{,}000{,}000mm^4} = 0.00687 \quad (7)$$

$$\Sigma\mu_H = N_c \text{ x } 4(M_e/M_p(P) - 1) = 3.3 \text{ x } 4(2.5 - 1) = 19.8 \quad (8)$$

$$\Delta_a = -0.5D\Sigma\mu_H\frac{\delta_p}{L} \quad (9)$$

= -0.5 x 390mm x 19.8 x 0.00687 = 26.5 mm

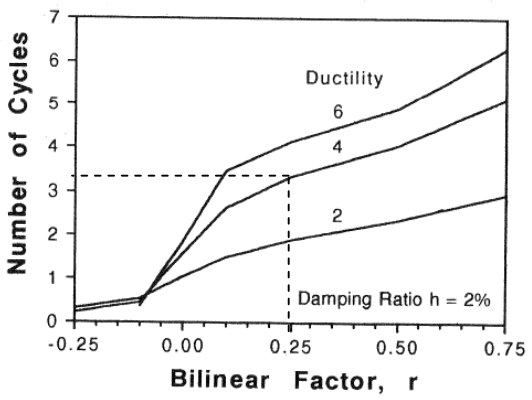

(a) Average for Different Ductilities

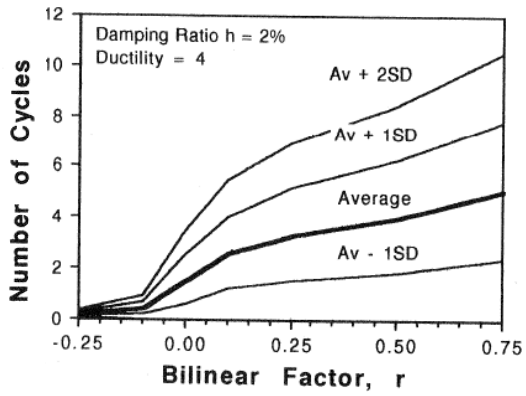

(b) Scatter for a Ductility of 4

Figure 16: Equivalent Number of Cycles - MacRae and Kawashima (1990).

c) Axial Shortening from Frame Inelastic Analysis

For computer software which considers inelastic rotation at a hinge, but which does not consider inelastic axial shortening, it is possible to obtain the moment-rotation behaviour at the base of yielding columns. The moment versus time plot can be developed. Since the moment cannot be greater than $M_p(P)$ for

elastic perfectly plastic response, the graph will be flat when it reaches this value. From each time-history analysis, the cumulative inelastic displacement, $\Sigma\mu_H\delta_p$, can be obtained from the moment-rotation hysteresis curve in the same manner as that obtained in Figure 6. This information can then be used in Equation 4 to obtain an estimate of the inelastic axial displacement.

d) Axial Shortening Estimate from Analysis Results

Equation 4 may be rewritten as Equation 10 where the left hand side of the equality is a non-dimensionalised inelastic axial shortening. Here, the ratio of d_p/L may be written as $M_p(P)L/(3EI)$, where E is the Young's modulus, I is the second moment of area for bending about the axis considered. The right hand side is a scaled cumulative inelastic ductility.

$$\frac{\Delta_a L}{D\left(\frac{P}{P_y}\frac{A}{A_w}\right)\delta_p} = -0.5\Sigma\mu_H \quad \text{for} \quad \frac{P}{P_y} \le \frac{A_w}{A}$$
$$\frac{\Delta_a L}{D\delta_p} = -0.5\Sigma\mu_H \quad \text{for} \quad \frac{P}{P_y} > \frac{A_w}{A} \qquad (10)$$

Again $\Sigma\mu_H$ may be found using Equation 8. Defining Δ_a^* in Equation 11 as a non-dimensional axial shortening ratio, it is possible to plot Δ_a^* against $M_e/M_p(P)$ as shown in Figure 17 for both design level and maximum credible level earthquakes. The value of P used to compute $M_p(P)$ was the maximum compressive value on the column. It would be expected that when $M_e/M_p(P)$ is less than unity, there would be no axial shortening. The value of P used in Equation 11 was the gravity axial force on the column. Scatter may be expected in the graph related to the equivalent number of cycles to which the earthquake subjects the column. There is a clear relationship between the parameters shown in Figure 17. The line shown in these diagrams is given in Equation 12. It gives an estimate of axial shortening which is slightly more conservative than the average.

$$\Delta_a^* = \begin{cases} \dfrac{\Delta_a L}{D\left(\frac{P}{P_y}\frac{A}{A_w}\right)\delta_p} & \text{for} \quad \dfrac{P}{P_y} \le \dfrac{A_w}{A} \\ \dfrac{\Delta_a L}{D\delta_p} & \text{for} \quad \dfrac{P}{P_y} > \dfrac{A_w}{A} \end{cases} \qquad (11)$$

$$\Delta^* = 3.5\,(M_e/M_p(P) - 1) \qquad (12)$$

As an example of the use of the graphs in Figure 17 for the prediction of axial shortening, consider the same column used in the previous example. Suppose that a comparison of elastic and inelastic analyses gave a moment ductility, $M_e/M_p\ (P)$, of 4. From Figure 17b and Equation 12, we obtain a value of non-dimensional axial shortening ratio, Δ^*, of 10.5. Knowing then that the ratio δ_p/L is equal to 0.00687 as found in Equation 7; that the depth, D, is 390 mm; and that the axial force ratio P/P_y is 0.4, the estimated axial shortening from Equation 13 is:

$$\Delta_a = \frac{\Delta_a{}^* \times D \times \delta_p}{L} = 10.5 \times 390 \times 0.00687 = 28.2mm \qquad (13)$$

Due to the scatter in data in Figure 17, this value may range from about 8mm to about 37.5 mm. This high degree of variability arises from the combined variability in axial force ratio and cumulative inelastic ductility. These are not considered in Figure 17, and the choice of best-fit line will influence predictions.

In the examples given above, the axial force ratio was assumed to remain constant. This may be reasonable for internal columns of moment frames when there are no vertical accelerations. However, column axial force generally changes with time during of the earthquake. This is especially true for EBF columns where the assumption of constant axial force is not reasonable and this is reflected in the lack of fit of the predicted curve from Equation 13 with the data shown in Figures 17 (a) and (b).

5. POSSIBLE MITIGATION METHODS

If column yielding can be mitigated, then axial shortening will also not occur. There are also other reasons for trying to prevent column yielding. These are listed below:

i) Column deformation capacity is lower than for beams because a larger proportion of the cross-section in compression, making it more susceptible to buckling failure. Also, larger strains occur in the extreme fibre of the section as illustrated in Figure 8. These strains cumulate under reversed inelastic cyclic loading as described above as a result of the axial shortening. MacRae *et al.* (1990) stated that the cumulative strain, which is related to the axial shortening, is what most significantly controls the lateral deformation capacity of columns. While the column element slenderness values may have been selected for non-uniform compression, the cyclic effects cause large cumulative strains over the whole section which may exacerbate strength loss due to buckling.

ii) Column unidirectional hinging may occur during reversed cycling as was found in an experimental study by Popov *et al.* (1975). This is shown for an internal column in a weak column strong beam frame in Figure 18. Here the column below the beam yields when the subassembly is pushed to the right, while that above the beam yields when pushed to the left as a result of strain hardening effects in the lower hinge. This means that the column is likely to deform into a C, or banana shape, when the loads are removed.

iii) Column yielding may lead to a soft story mechanism

iv) Column strength loss may be catastrophic, and

v) Column yielding may cause undesirable frame effects associated with axial shortening.

Three methods of preventing yielding at the base of steel columns are discussed below. These methods dissipate hysteretic energy using mechanisms other than column yielding. A fourth method, which aims to reduce inelastic axial displacements, is also presented.

a) The double friction (DF) concept is a generalization of the sliding hinge joint (SHJ) concept originally developed for steel beam-column connections by Clifton (2005). The SHJ joint is known as a Generation 4 joint (Mackinven 2007) because it dissipates energy without significant extension of the slab above the beam, and without beam growth. The concept has recently been used by Connell-Wagner at the base of ground storey columns of two 11-storey buildings and one five-storey building designed for Wellington (Gledhill *et al.,* 2008).

A conceptual drawing of a DF base connection, different to the Connell-Wagner one is given in Figure 19a. Here, axial force is transferred directly from the column to the pin at the centre of the column to the foundation. Shear force is carried the same way. Flexure is carried by means of friction between the beam flange and the foundation flange plate. Slotted holes in the foundation flange plate allow the beam flange to sustain large deformations. A floating plate on the

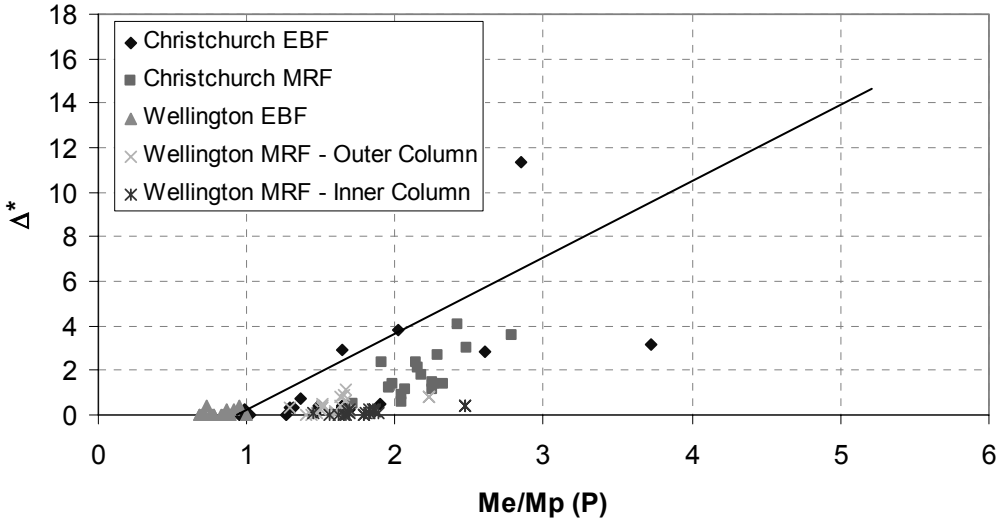

(a) 500 year Event

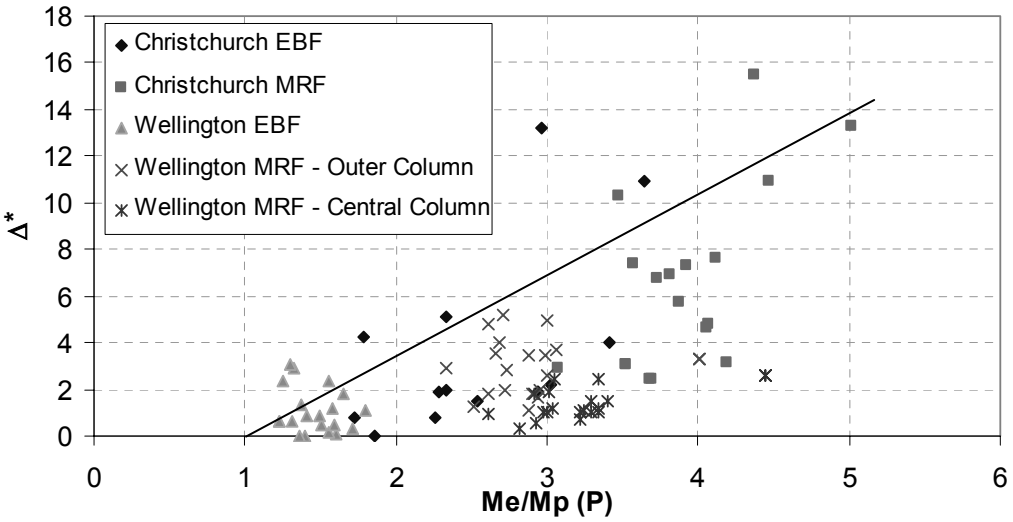

(b) 2500 year Event

Figure 17: Axial Shortening ratio, Δ*, vs. $M_e/M_p(P)$.

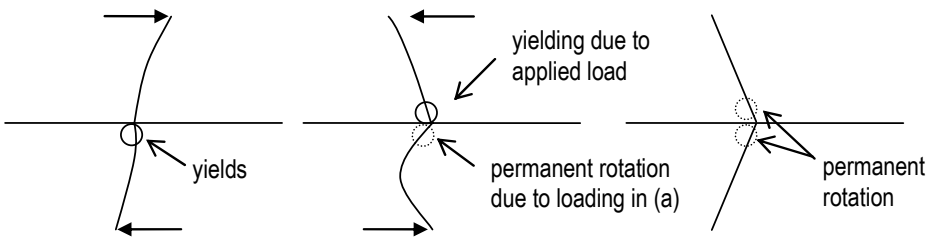

(a) loading to right *(b) loading to left* *(c) After load removal*

Figure 18. Column Unidirectional Hinging.

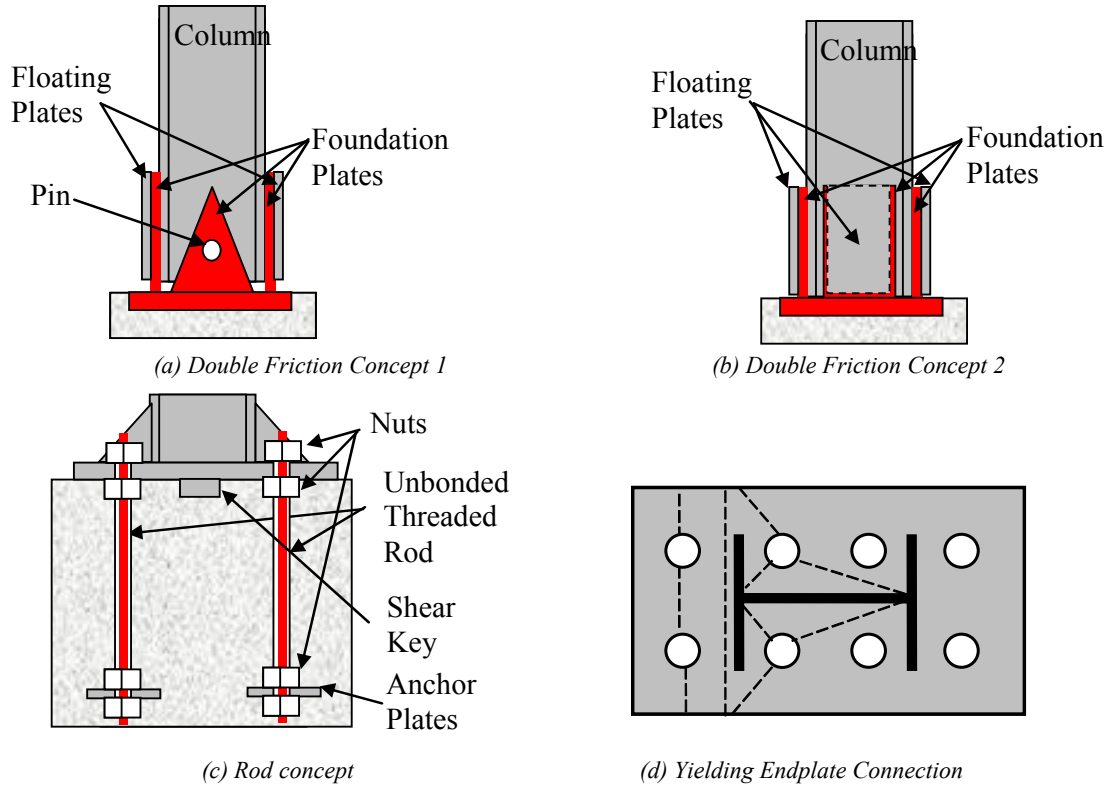

(a) Double Friction Concept 1

(b) Double Friction Concept 2

(c) Rod concept

(d) Yielding Endplate Connection

Figure 19: Some Possible Methods for Preventing Column Yielding.

outside of the foundation flange plate is connected only by bolts to the beam flange through the foundation flange plate slotted holes. This means that as the beam flange moves relative to the foundation flange plate, it also drags the floating plate with it creating friction on two surfaces on each flange and hence the double friction (DF) terminology. After the shaking there is almost no permanent damage. The joint has been shown to be a very desirable method for resisting earthquake action.

An alternative DF connection is given in Figure 19b. Here the column sits on top of the foundation without direct connection except through the bolts to the foundation flange plates and foundation web plate. The flange plates are detailed as before, and the web plate has vertical elongated holes in it with bolts passing through it so that sliding friction may be developed between the foundation web plate and beam web, as well as between the foundation web plate and floating web plate shown on the opposite side of the foundation web plate to the beam web. Column axial compression goes directly from the column into the foundation and shear is carried through the bolts in the web. If the column is subject to large axial tension, it will be designed to stop moving when the bolts hit the top end of the elongated holes in the foundation plates. This detail is easier to construct than the first, but one side of the column has to move up (much like a concrete column) to allow flexural deformation to occur. This changes the height of the centre of the column. There is also the possibility that after a major earthquake that the column may not have returned to its initial position, so the bolts may need to be loosened and tightened again.

Further details on the DF and SHJ concept are described by Clifton (2005) and Mackinven *et al.* (2007).

b) Another damage free connection at the base of steel columns was presented by Mackinven *et al.* (2007). This connection, shown in Figure 19c, involves the use of unbonded steel rods to act as re-centring devices while the steel column rocks under lateral loads. The unbonded length of the rods is sufficient to allow elastic extension to re-centre the rocking column. The rod has a specifically detailed thread passing through it and a nut above and below the end plate. Such a thread can withstand many cycles without fracturing. As above, the absence of yielding in the column results in the elimination of inelastic axial shortening.

c) A third method of preventing yielding in the base of the column, and hence axial shortening, is to use a yielding endplate connection, shown in Figure 19d. Using yield line theory, a yielding mechanism of the plate can be found and considered in design. By concentrating yielding in the end plate, compressive yielding may be prevented in the column.

A method to mitigate axial shortening, while still permitting column yielding, is shown in Figure 20 (Hyde, 2006). Here, an extra area of steel at mid-section is sufficiently sized to carry the total axial force in the column. By doing this, the position of the neutral axis is restricted to the central stiffener under service loads, and inelastic displacement is insufficient to cause significant shortening. The extra steel does not significantly change the moment capacity under no axial force, but it does change the moment axial force interaction diagram, as shown in Figure 20d, such that the moment capacity is not likely to be sensitive to axial force. Although the method was shown to greatly reduce the amount of axial shortening in columns, it is fairly expensive to implement. An investigation on partial height stiffeners was also conducted. The stiffeners were continued to the section depth above where the yield moment in the bare column could occur. Also, tapering of the stiffener was considered to reduce stresses due to the significant change in stiffness in the column at the top of the stiffener. It was found that as soon as beam web buckling was initiated, the column moved sideways due to the cyclic loading and yielding above the

stiffener occurred thereby resulting in unsatisfactory behaviour. For this reason, partial height stiffeners of this form are not recommended.

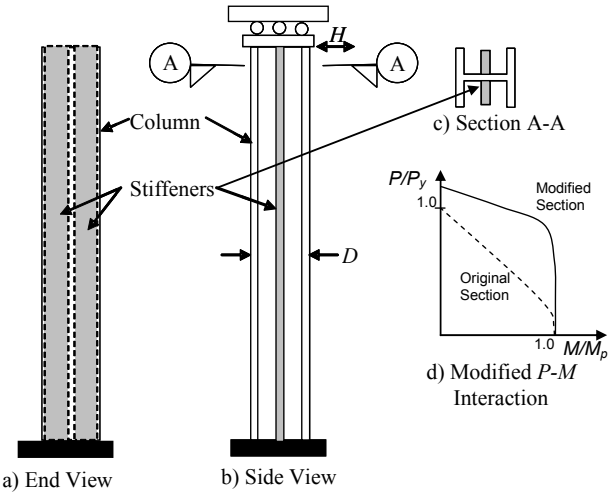

Figure 20: Full Height Stiffener (Hyde, 2006.)

CONCLUSIONS

This paper describes experimental and analytical studies on the axial shortening of columns in steel frames as a result of inelastic earthquake excitation. It is shown that:

i) Axial shortening of steel columns subject to monotonic or cyclic loading can occur due to nonlinear material effects without any section or member buckling. Buckling tended to exacerbate the shortening after an axial displacement of about 2% of the member depth in the compact members tested.

ii) A simple model relating the axial shortening due to material effects was developed as a function of cumulative inelastic rotation, axial force level and member depth.

iii) A fibre joint for a frame program was developed which considered axial shortening.

iv) Two moment frames and two eccentrically-braced frames designed for regions of moderate and high seismicity were analysed using the fibre joint. The average axial displacement at the base of the most critical column of the most critical MRF was 4.3 mm, and it was 1.9 mm for the EBF from 20 design level earthquake records. These values were 17.0 mm and 3.4 mm for the critical MRF and EBF column respectively for maximum credible level shaking.

v) Methods to estimate the amount of axial shortening in a steel frame were developed based on the assumption that columns were subject to constant axial force during the shaking.

vi) Possible methods to mitigate axial shortening were described.

REFERENCES

ABAQUS Inc. (2004). *ABAQUS* (Version 6.5.1) [Computer Software]. Providence

Carr, A.J. (2007). *Ruaumoko-2D* [Computer Software]. Department of Civil Engineering, University of Canterbury, Christchurch

Clifton, G.C. (2005). "Semi-Rigid Joints for Moment Resisting Steel Framed Seismic Resisting Systems". PhD Thesis, *Department of Civil and Environmental Engineering,* University of Auckland.

Gledhill, S.M., Sidwell, G.K., and Bell, D.K. (2008). "The Damage Avoidance Design of tall steel frame buildings - Fairlie Terrace Student Accommodation Project, Victoria University of Wellington", *New Zealand Society of Earthquake Engineering Annual Conference*, Wairakei, April.

Hyde, K., MacRae, G.A., Moss, P.J. and Walpole, W.R. (2006). "Axial Shortening of Steel Columns Subjected to Constant Axial Compression and Inelastic Cyclic Displacements". Research Report 06-6, *Department of Civil Engineering, University of Canterbury*, Christchurch.

Hopperstad, O.S. and Remseth, S. (1996). "On Cyclic Stability of Beam-Columns". XXV General Assembly of the European Seismology Commission (Ed. Thorkelsson, B.).

Mackinven, H., MacRae, G.A., Pampanin, S., Clifton, G.C. and Butterworth, J. (2007). "Generation Four Steel Moment Frame Joints". *Pacific Conference on Earthquake Engineering.*

MacRae, G.A., Carr, A.J. and Walpole, W.R. (1990). "The Seismic Response of Steel Frames". Research Report 90-6, *Department of Civil Engineering, University of Canterbury,* Christchurch

MacRae, G. A. and Kawashima, K. (1993). "The Seismic Response of Bilinear Oscillators using Japanese Earthquake Records". Journal of Research, Vol. 30, *Public Works Research Institute, Ministry of Construction, Ibaraki*.

Peng, B., MacRae, G., Walpole, W., Moss, P. and Dhakal, R., "Plastic Hinge Location in Columns of Steel Frames", *Civil Engineering Research Report*, *University of Canterbury,* 2006-05. ISSN 0110-3326. June 2006.

Popov, E. P., Bertero, V. V. and Chandramoulli, S., (1975). "Hysteretic Behaviour of Steel Columns", UCB/EERC 75-11, *Earthquake Engineering Research Centre,* Richmond, USA.

Somerville, P., Smith, N., and Penyamurthula, S., "Development of Ground Motion Time Histories for Phase II of the FEMA/SAC Steel Project", *SAC Background Document Report,* Report No. SAC/BD-97/04, 1997.

Standards New Zealand (1997). *NZS 3404: 1997 Steel Structures Standard*. Standards New Zealand, Wellington.

Standards New Zealand (2002). *AS/NZS 1170: 2004 Structural Design Actions*. Standards New Zealand, Wellington.

ACKNOWLEDGEMENTS

The authors wish to thank both the Heavy Engineering Research Association (HERA), and the Steel Construction New Zealand (SCNZ) for financially supporting this project and to acknowledge Xiao Huantian of SCNZ for providing the frames used in the analyses. All opinions expressed are those of the authors and do not necessarily reflect those of the funding agencies.